

Physical Interactions between Mcm10, DNA, and DNA Polymerase α ^{*S}

Received for publication, May 13, 2009, and in revised form, June 29, 2009. Published, JBC Papers in Press, July 16, 2009, DOI 10.1074/jbc.M109.020438

Eric M. Warren^{†S1}, Hao Huang[‡], Ellen Fanning[‡], Walter J. Chazin^{S¶}, and Brandt F. Eichman^{†S¶2}

From the [†]Department of Biological Sciences, the [¶]Department of Biochemistry, and the ^SCenter for Structural Biology, Vanderbilt University, Nashville, Tennessee 37232

Mcm10 is an essential eukaryotic protein required for the initiation and elongation phases of chromosomal replication. Specifically, Mcm10 is required for the association of several replication proteins, including DNA polymerase α (pol α), with chromatin. We showed previously that the internal (ID) and C-terminal (CTD) domains of Mcm10 physically interact with both single-stranded (ss) DNA and the catalytic p180 subunit of pol α . However, the mechanism by which Mcm10 interacts with pol α on and off DNA is unclear. As a first step toward understanding the structural details for these critical intermolecular interactions, x-ray crystallography and NMR spectroscopy were used to map the binary interfaces between Mcm10-ID, ssDNA, and p180. The crystal structure of an Mcm10-ID-ssDNA complex confirmed and extended our previous evidence that ssDNA binds within the oligonucleotide/oligosaccharide binding-fold cleft of Mcm10-ID. We show using NMR chemical shift perturbation and fluorescence spectroscopy that p180 also binds to the OB-fold and that ssDNA and p180 compete for binding to this motif. In addition, we map a minimal Mcm10 binding site on p180 to a small region within the p180 N-terminal domain (residues 286–310). These findings, together with data for DNA and p180 binding to an Mcm10 construct that contains both the ID and CTD, provide the first mechanistic insight into how Mcm10 might use a handoff mechanism to load and stabilize pol α within the replication fork.

To maintain their genomic integrity, cells must ensure complete and accurate DNA replication once per cell cycle. Consequently, DNA replication is a highly regulated and orchestrated series of molecular events. Multiprotein complexes assembled at origins of replication lead to assembly of additional proteins that unwind chromosomal DNA and synthesize nascent

strands. The first event is the formation of a pre-replicative complex, which is composed of the origin recognition complex, Cdc6, Cdt1, and Mcm2–7 (for review, see Ref. 1). Initiation of replication at the onset of S-phase involves the activity of cyclin- and Dbf4-dependent kinases concurrent with recruitment of key factors to the origin. Among these, Mcm10 (2, 3) is recruited in early S-phase and is required for loading of Cdc45 (4). Mcm2–7, Cdc45, and the GINS complex form the replicative helicase (5–8). Origin unwinding is followed by loading of RPA,³ And-1/Ctf4, and pol α onto ssDNA (9–12). In addition, recruitment of Sld2, Sld3, and Dpb11/TopBP1 are essential for replication initiation (13, 14), and association of topoisomerase I, proliferating cellular nuclear antigen (PCNA), replication factor C, and the replicative DNA polymerases δ and ϵ completes the replisome (for review, see Ref. 15).

Mcm10 is exclusive to eukaryotes and is essential to both initiation and elongation phases of chromosomal DNA replication (6, 8, 16). Mutations in Mcm10 in yeast result in stalled replication, cell cycle arrest, and cell death (2, 3, 17–19). These defects can be explained by the number of genetic and physical interactions between Mcm10 and many essential replication proteins, including origin recognition complex, Mcm2–7, and PCNA (3, 12, 20–24). In addition, Mcm10 has been shown to stimulate the phosphorylation of Mcm2–7 by Dbf4-dependent kinase *in vitro* (25). Thus, Mcm10 is an integral component of the replication machinery.

Importantly, Mcm10 physically interacts with and stabilizes pol α and helps to maintain its association with chromatin (16, 26, 27). This is a critical interaction during replication because pol α is the only enzyme in eukaryotic cells that is capable of initiating DNA synthesis *de novo*. Indeed, Mcm10 stimulates the polymerase activity of pol α *in vitro* (28), and interestingly, the fission yeast Mcm10, but not *Xenopus* Mcm10, has been shown to exhibit primase activity (29, 30). Mcm10 is composed of three domains, the N-terminal (NTD), internal (ID), and C-terminal (CTD) domains (29). The NTD is presumably an oligomerization domain, whereas the ID and CTD both interact with DNA and pol α (29). The CTD is not found in yeast, whereas the ID is highly conserved among all eukaryotes. The crystal structure of Mcm10-ID showed that this domain is com-

* This work was supported, in whole or in part, by National Institutes of Health Grants R01 GM080570 (to B. F. E.), R01 GM65484 (to W. J. C.), and R01 GM52948 (to E. F.). Additional support for crystallography and mass spectrometry facilities was provided by the Vanderbilt Center in Molecular Toxicology (National Institutes of Health Grant P30 ES000267) and the Vanderbilt-Ingram Cancer Center (National Institutes of Health Grant P30 CA068485).

^S The on-line version of this article (available at <http://www.jbc.org>) contains supplemental Figs. S1–S9.

The atomic coordinates and structure factors (code 3H15) have been deposited in the Protein Data Bank, Research Collaboratory for Structural Bioinformatics, Rutgers University, New Brunswick, NJ (<http://www.rcsb.org/>).

¹ Supported in part by Molecular Biophysics Training Grant T32 GM08320.

² To whom correspondence should be addressed: VU Station B, Box 351634, Nashville, TN 37235-1634. Fax: 615-343-6707; E-mail: brandt.eichman@vanderbilt.edu.

³ The abbreviations used are: RPA, replication protein A; pol, polymerase; NTD, N-terminal domain; ID, internal domain; CTD, C-terminal domain; OB, oligonucleotide/oligosaccharide binding; TAPS, 3-[[2-hydroxy-1,1-bis(hydroxymethyl)ethyl]amino]-1-propanesulfonic acid; GST, glutathione S-transferase; ssDNA, single-stranded DNA; dsDNA, double-stranded DNA; PCNA, proliferating cellular nuclear antigen; HSQC, heteronuclear single quantum correlation.

posed of an oligonucleotide/oligosaccharide binding (OB)-fold and a zinc finger motif, which form a unified DNA binding platform (31). An Hsp10-like motif important for the interaction with pol α has been identified in the sequence of *Saccharomyces cerevisiae* Mcm10-ID (16, 26).

DNA pol α -primase is composed of four subunits: p180, p68, p58, and p48. The p180 subunit possesses the catalytic DNA polymerase activity, and disruption of this gene is lethal (32, 33). p58 and p48 form the DNA-dependent RNA polymerase (primase) activity (34, 35), whereas the p68 subunit has no known catalytic activity but serves a regulatory role (36, 37). Pol α plays an essential role in lagging strand synthesis by first creating short (7–12 nucleotide) RNA primers followed by DNA extension. At the critical length of \sim 30 nucleotides, replication factor C binds to the nascent strand to displace pol α and loads PCNA with pols δ and ϵ (for review, see Ref. 38).

The interaction between Mcm10 and pol α has led to the suggestion that Mcm10 may help recruit the polymerase to the emerging replisome. However, the molecular details of this interaction and the mechanism by which Mcm10 may recruit and stabilize the pol α complex on DNA has not been investigated. Presented here is the high resolution structure of the conserved Mcm10-ID bound to ssDNA together with NMR chemical shift perturbation competition data for pol α binding in the presence of ssDNA. Collectively, these data demonstrate a shared binding site for DNA and pol α in the OB-fold cleft of Mcm10-ID, with a preference for ssDNA over pol α . In addition, we have mapped the Mcm10-ID binding site on pol α to a 24-residue segment of the N-terminal domain of p180. Based on these results, we propose Mcm10 helps to recruit pol α to origins of replication by a molecular hand-off mechanism.

EXPERIMENTAL PROCEDURES

Protein Expression and Purification—Mcm10-ID was prepared as described previously (31). Briefly, the protein was overexpressed from a modified pET-32a vector (Novagen) in *Escherichia coli* BL21(DE3) cells for 16 h at 16 °C and isolated using nickel affinity chromatography. After cleavage of the thioredoxin-His₆ tag, Mcm10-ID was purified using ssDNA affinity and size exclusion chromatography. An Mcm10 construct spanning amino acid residues 230–860 (Mcm10-ID+CTD) was cloned and expressed similarly to Mcm10-ID, except protein expression was induced at 21 °C for 4 h. Mcm10-ID+CTD protein was purified by nickel-nitrilotriacetic acid affinity chromatography (Qiagen) followed by S-Sepharose (GE Healthcare) ion exchange chromatography and cleavage of the affinity tag. The cleaved protein was further purified by gel filtration using a Superdex 200 preparative column (GE Healthcare) equilibrated in 20 mM Tris, pH 7.5, 150 mM NaCl, 3.5 mM β -mercaptoethanol, and 5% glycerol (buffer A).

The DNA encoding amino acids 189–323 of human p180 was ligated into a modified pET-27 vector (Novagen) to produce an N-terminal His₆ fusion protein (pBG100, Vanderbilt Center for Structural Biology). *E. coli* BL21(DE3) cells transformed with the p180^{189–323}/pBG100 plasmid were grown at 37 °C in LB medium containing 100 μ g/ml ampicillin, and protein was overexpressed by the addition of 0.5 mM isopropyl 1-thio- β -D-galactopyranoside for 4 h. For NMR experiments,

protein was uniformly enriched with ¹⁵N by propagating cells in M9 minimal medium supplemented with 1 mg/ml ¹⁵NH₄Cl (Cambridge Isotope Laboratories) as the sole source of nitrogen. The cells were harvested in 50 mM Tris, pH 7.5, 500 mM NaCl, and 10% glycerol and lysed under pressure (25,000 p.s.i.) using an Avestin EmulsiFlex C3 homogenizer. p180^{189–323} was purified by nickel-nitrilotriacetic acid affinity chromatography (Qiagen) followed by cleavage of the affinity tag. The cleaved protein was further purified by Q-Sepharose (GE Healthcare) ion exchange chromatography followed by gel filtration using a Superdex 200 preparative column (GE Healthcare) equilibrated in buffer A. p180^{243–256} and p180^{286–310} peptides used for NMR titrations were synthesized and purified by Genescript Corp. (Piscataway, NJ).

X-ray Crystallography—Crystals were grown by sitting drop vapor diffusion by mixing 2 μ l of protein/DNA solution containing 300 μ M Mcm10-ID and 360 μ M dC₉ ssDNA with 2 μ l of reservoir solution containing 100 mM TAPS, pH 9.0, and 17% polyethylene glycol 3350. Crystals appeared overnight and grew to \sim 50 \times 50 \times 200 μ m³ after 2–3 days. Crystals were soaked for 5 min in mother liquor containing 10% (v/v) butanediol and flash-frozen in liquid nitrogen. Preliminary x-ray diffraction data (Table 1) were collected at beamline 21-ID at the Advanced Photon Source (Argonne, IL) and processed with HKL2000 (39). The Mcm10-ID:ssDNA complex crystallized in space group P3₁21 with one molecule in the asymmetric unit.

X-ray phases were obtained by molecular replacement using unliganded Mcm10-ID (PDB code 3EBE) as the search model in the program Molrep (40). A clear rotation/translation solution was verified by the quality of the resulting composite annealed $2F_o - F_c$ omit electron density maps generated using CNS (41) (supplemental Fig. S1). Several iterative rounds of restrained atomic and temperature factor refinement against a maximum likelihood crystallographic target in Phenix (42) together with manual model adjustment and building the L12 loop in Coot (43) resulted in R and R_{free} values of 21.7 and 26.1%, respectively. Strong $F_o - F_c$ difference Fourier density was observed within the OB-fold cleft (residues 292–360). Three nucleotides of ssDNA were fit into this density using Coot and refined, which lowered R and R_{free} by 0.8 and 1.61%, respectively. The polarity of the DNA was established by parallel refinement of both orientations of DNA, which differed from each other by 1% in R_{free} . Translation/libration/screw refinement was used to model anisotropic motion of 6 groups, defined by protein residues 235–241, 242–260, 261–300, 301–371, 372–500, and DNA as determined by the TLSMD server (44). Individual anisotropic B-factors were derived from the refined translation/libration/screw parameters and held fixed during subsequent rounds of refinement, which resulted in a noticeable improvement of the electron density maps (supplemental Fig. S1) and a 1% decrease in both R and R_{free} . No additional electron density was discerned corresponding to the six remaining nucleotides or for residues 230–231 and 416–427 at the extreme N and C termini.

Analysis of the final structure using PROCHECK (45) showed 80.5 and 19.5% of the total of 154 non-glycine and non-proline residues to be within the most favored and allowed regions of the Ramachandran plot, respectively, with no resi-

Interactions between Mcm10, DNA, and Pol α

dues in the disallowed region. The coordinates and structure factors have been deposited in the Protein Data Bank under accession number 3H15.

NMR Spectroscopy—Gradient-enhanced ^1H , ^{15}N HSQC NMR spectra were recorded at 25 °C using a Bruker DRX 800 NMR spectrometer equipped with single axis z-gradient cryoprobe. All spectra were acquired with 1024 complex points over a sweep width of 15 ppm in the ^1H dimension and 128 complex points over 37 ppm in the ^{15}N dimension. The center of the ^{15}N spectral width was set to 117.5 ppm, and the ^1H carrier was placed on the water signal at 4.7 ppm from the respective base spectrometer frequencies. All spectra were processed and analyzed using Topspin v1.3 (Bruker, Billerica, MA) and Sparky version 3.1 (University of California, San Francisco, CA). Data were treated with shifted sine-bell functions and zero-filled to twice the number of data points in both dimensions.

Chemical shift perturbation data were collected by titrating 1.8 mM unlabeled p180^{189–323} into 400 μM ^{15}N -labeled Mcm10-ID in 20 mM Tris-d₁₁, pH 7.0, 75 mM NaCl, and 5% D₂O. Additionally, unlabeled Mcm10-ID was titrated into 400 μM ^{15}N -labeled p180^{189–323} in the same buffer. Both the salt concentration and temperature for the NMR experiment were optimized in all cases to be as close as possible to physiological conditions, within the limit of ensuring acceptable sensitivity. Spectra were recorded at Mcm10-ID:p180^{189–323} ratios of 1:0, 1:0.25, 1:0.63, 1:1, and 1:2. The 15-mer oligonucleotide d(GGCGCATTGTCGCAA) was used for ssDNA titrations and was previously verified by UV spectroscopy to be single-stranded under the conditions tested (31). The observation of chemical shift perturbations in the fast-to-intermediate exchange regime (on the NMR time scale) enabled most of the peaks in the free protein and complexes to be correlated. In cases where the peaks disappeared, the last titration point where the peak was observed was used for determining chemical shift perturbations. The magnitudes of the average chemical shift (δ) perturbations shown in Fig. 3B and supplemental Figs. S7B and S8A were calculated from contributions of both ^{15}N and ^1H dimensions in the HSQC spectrum by using the equation, $\Delta\delta_{\text{ave}} = (((\Delta\delta_{1\text{H}})^2 + (\Delta\delta_{15\text{N}}/5)^2)/2)^{1/2}$.

Fluorescence Anisotropy—Mcm10-ID and Mcm10-ID+CTD binding to p180 and DNA was measured by following an increase in fluorescence anisotropy as unlabeled Mcm10 domains were added to fluorescein labeled p180 fragments and oligonucleotides. Fluorescein-p180^{189–323} was prepared by incubating purified p180^{189–323} with a 20-fold molar excess of MTS-fluorescein (2-[(5-fluoreceinyl) aminocarbonyl]ethyl methanethiosulfonate, Toronto Research Chemicals) at 25 °C for 6 h followed by purification on a 1-ml Q-Sepharose column (GE Healthcare). Fluorescein isothiocyanate-conjugated p180^{286–310} was synthesized and purified by Genescript Corp., and oligonucleotides containing 3'-labeled 6-carboxyfluorescein were synthesized by Integrated DNA Technologies. All binding and competition reactions were carried out at 25 °C in 20 mM Tris, pH 7.5, 150 mM NaCl, and 5% glycerol. Polarized fluorescence intensities were measured at excitation and emission wavelengths of 495 and 538 nm, respectively. For binding measurements, unlabeled Mcm10 protein was added over a concentration range of 0.1–50 μM to solutions containing

either 50 nM fluorescein-p180 fragment or 50 nM fluorescein-DNA. Dissociation constants (K_d) were derived by fitting a two-state binding model to data from three experiments using Kaleidagraph 3.6 (Synergy Software) according to the equation $r = r_o + (r_{\text{max}} - r_o) ([\text{Mcm10}]/(K_d + [\text{Mcm10}]))$, where r is the fluorescence anisotropy, and r_o and r_{max} are the anisotropy values of unbound and fully bound DNA, respectively. For competition reactions, 15 μM Mcm10-ID was preincubated for 30 min with 50 nM fluorescein-p180^{189–323} or 50 nM fluorescein-ssDNA 25-mer (nucleotide sequence shown in Table 2). Under these conditions, both fluorescein-labeled molecules are >80% saturated (Fig. 2B and Ref. 31). The presence of free fluorescein-labeled ssDNA and p180^{189–323} does not interfere with the measurement because p180^{189–323} and ssDNA do not interact (Fig. 2B). Unlabeled ssDNA-25-mer or p180^{189–323} was added over a concentration range of 1–250 μM , and the decay in anisotropy was monitored. EC₅₀ value was determined by fitting the equation $r = -r_o - (r_{\text{max}} - r_o) ([\text{competitor}]/(\text{EC}_{50} + [\text{competitor}]))$, and the K_i were determined according to the equation $K_i = \text{EC}_{50}/(1 + ([\text{Mcm10}]/K_d))$.

Isothermal Titration Calorimetry—Proteins were buffer-exchanged into 25 mM Tris, pH 7.5, and 100 mM NaCl and concentrated to 50 μM (Mcm10-ID) and 1 mM (p180^{189–323}). 1.7 ml of Mcm10-ID was placed in the sample cell, into which p180^{189–323} was injected in 6- μl steps during the run. Data were collected at 25 °C using a MicroCal VP-isothermal titration calorimetry and analyzed using the accompanying Origin software (Origin Lab, Northampton, MA). Thermodynamic parameters were calculated from fitting the data to the best binding model using Origin according to the Gibbs free energy equation, $\Delta G = \Delta H - T\Delta S = -RT\ln K_d$.

RESULTS

The Crystal Structure of Mcm10-ID Bound to ssDNA—The highly conserved internal domain of *Xenopus laevis* Mcm10 (Mcm10-ID) has previously been suggested to bind DNA along the surface formed by the concave OB-fold β -barrel and the extended zinc finger loop (31). To elucidate the details of the Mcm10-ID:ssDNA interaction at high resolution, we determined the crystal structure of Mcm10-ID in complex with ssDNA using the unliganded Mcm10-ID structure as a molecular replacement search model (Fig. 1). Strong electron density corresponding to three consecutive cytidine nucleotides of ssDNA was clearly visible inside the OB-fold cleft (Fig. 1A), similar to the location of bound ssDNA in OB-fold structures of RPA, Rho, RecG, and RumA (46–50). These proteins typically bind ssDNA between the OB-fold L12 and L45 loops, which are often flexible in the absence of DNA (51). Consistent with other OB-fold:ssDNA complexes, Mcm10-ID L12 loop (residues 297–305), which was not observed in the unliganded structure, is now visible in the complex as the flexibility of this loop is quenched by interactions with the DNA (Fig. 1B). The atomic model for Mcm10-ID:ssDNA was refined to 2.7 Å to a crystallographic residual of 19.7% ($R_{\text{free}} = 23.2\%$). Data collection and refinement statistics are shown in Table 1.

The electron density for the ssDNA traverses β -strands β 1- β 3 and β 5.1, which form the concave surface of the OB-fold cleft (Fig. 1A). The polarity of the DNA is such that the 5'-end

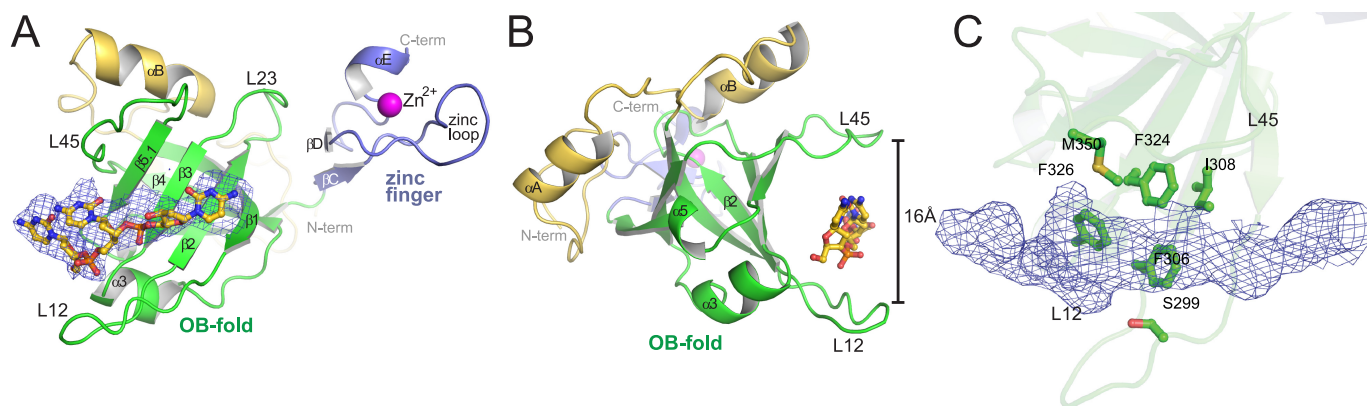


FIGURE 1. Crystal structure of Mcm10-ID bound to ssDNA. *A*, the crystal structure of Mcm10-ID bound to ssDNA is shown as a ribbon representation. The various protein structural motifs are colored to distinguish the N-terminal helical region (gold), the OB-fold (green), and the zinc-finger (blue protein and magenta zinc). The secondary structural elements are labeled as previously designated (31). The DNA molecule is rendered as yellow sticks and fit to annealed omit electron density contoured at 3σ . *B*, a side view of panel *A* illustrates the closing of loops L12 and L45 in the presence of ssDNA. *C*, close-up of the DNA binding site. The annealed omit electron density shows the location of the ssDNA. Mcm10-ID side chains contacting the DNA are rendered as sticks.

TABLE 1
Data collection and refinement statistics for Mcm10-ID-ssDNA complex

Values in parentheses are for highest resolution shell.

Data collection	
Space group	P3 ₁ 21
Cell dimensions	
<i>a</i> , <i>b</i> , <i>c</i> (Å)	95.02, 95.02, 61.16
α , β , γ (°)	90, 90, 120
Resolution (Å)	50.0-2.72 (2.72)
R_{sym}	8.2 (30.5)
$I/\sigma(I)$	11.38 (1.55)
Completeness (%)	90.2 (51.4)
Redundancy	5.3 (2.1)
Refinement	
Resolution (Å)	2.72
No. reflections	8221
$R_{\text{work}}/R_{\text{free}}$	0.197/0.232
No. atoms	
Protein	1395
DNA	54
Water	15
<i>B</i> -factors	
Protein	80.1
DNA	171.3
Water	69.3
Root mean square deviations	
Bond lengths (Å)	0.007
Bond angles (°)	1.245

starts at the $\beta 5.1$ strand and the 3'-end points toward $\beta 1$ and the zinc finger in a similar manner to the RPA70AB-ssDNA complex (46). Refining the DNA in the opposite orientation had a detrimental impact on the crystallographic residual. The L12 and L45 loops wrap around the DNA, creating a channel ~ 16 Å in diameter (Fig. 1*B*). Polar and hydrophobic side chains from both loops and lining the β -sheet make van der Waals contact with the DNA, including Ser-299, Phe-306, Ile-308, Phe-324, Phe-326, Met-350, and Lys-353 (Fig. 1*C* and supplemental Fig. S2). The high *B*-factors for the DNA (Table 1) indicate that the DNA is highly mobile and somewhat disordered within this hydrophobic cleft, which precludes our ability to precisely model the DNA atoms that contact the protein. Nonetheless, the DNA binding surface on the protein and the polarity of the DNA are clearly defined. Electron density was not observed for the DNA around the zinc finger, presumably because of steric occlusion of the zinc finger binding site due to crystal packing. In this crystal form, the L45 loop of a neighboring molecule

protrudes into the cleft between the OB-fold and the zinc finger, blocking ssDNA access to the zinc finger (supplemental Fig. S3). Although the entire DNA molecule cannot be identified from the present crystallographic data, this result confirms previous evidence that ssDNA binds directly to the OB-fold cleft (31) and is consistent with the orientation of DNA observed in other OB-folds (46–48).

The structure of ssDNA-bound Mcm10-ID is nearly identical to the unliganded structure previously published with root mean square deviation of 0.77 Å for all *C* α atoms (31). Apart from the now-ordered L12 DNA binding loop, the only notable difference between the two structures lies at the zinc finger helix at the extreme C terminus of the ID (residues 405–416). This helix is well defined in the unliganded protein and is engaged in intermolecular protein-protein contacts in each of the three protomers in the asymmetric unit (supplemental Fig. S4) (31). In the complex, which crystallizes in a different lattice with one protein-DNA complex per asymmetric unit, the zinc finger helix is disordered past the Zn^{2+} -coordinating His-406. This local unfolding is presumably because of the lack of any intermolecular contacts in the present crystal lattice and suggests that the fold of this helix in the full-length protein may be stabilized through protein contacts outside of the ID.

Mcm10-ID Binds to p180^{189–323}—Mcm10-ID has previously been shown to bind to the N-terminal 323 residues of the p180 subunit of human pol α -primase (29). This region is highly conserved but lacks appreciable predicted secondary structure or sequence complexity. To map the Mcm10-p180 interaction in detail, p180^{1–323} was subjected to limited proteolysis, and the resulting stable fragments were identified by mass spectrometry. Proteolytically sensitive sites were found at residues 145 and 189. Consequently, p180^{1–145} and p180^{189–323} were subcloned, purified, and tested for physical interaction with Mcm10-ID by affinity chromatography pulldown assays. The p180^{1–145} protein was not sufficiently stable in solution to test for a putative interaction. However, GST-tagged p180^{189–323} immobilized on glutathione-Sepharose was able to capture His-tagged Mcm10-ID from solution (Fig. 2*A*), demonstrating that this region of the p180 subunit is sufficient to bind to Mcm10-

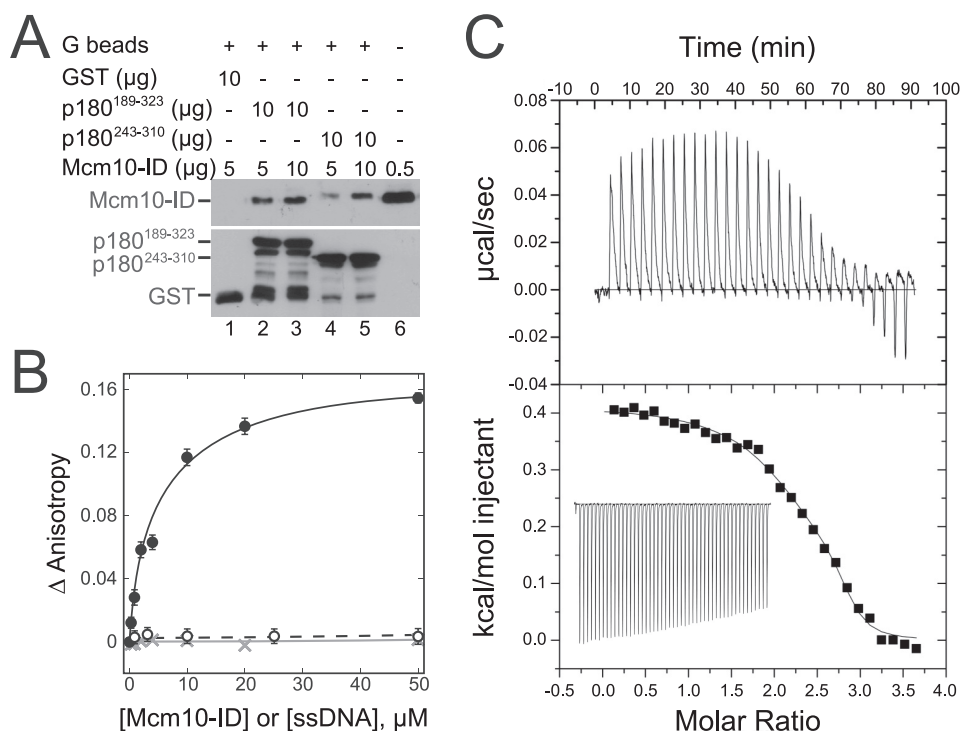


FIGURE 2. p180¹⁸⁹⁻³²³ physically interacts with Mcm10-ID. *A*, affinity capture experiments between His-tagged Mcm10-ID and GST-tagged p180 fragments. p180 fragments 189–323 and 243–310 were adsorbed on glutathione (G) beads and mixed with Mcm10-ID in the amounts indicated. Bound Mcm10-ID was detected by Western blotting with α -His antibody (upper blot), whereas retention of p180 fragments was detected by Western blotting with α -GST antibodies (lower blot). *B*, protein-protein binding was monitored by following a change in fluorescence anisotropy as Mcm10-ID (closed circles) or 25-mer ssDNA (open circles) was titrated into a solution containing fluorescein-labeled p180¹⁸⁹⁻³²³. A control in which only buffer was added in the same volume as in the Mcm10 titration is also shown (crosses). Error bars represent the S.D. from the average values from three independent measurements. The dissociation constant (K_d) for Mcm10-ID binding to p180¹⁸⁹⁻³²³ was determined to be $12 \pm 2 \mu$ M as described under “Experimental Procedures.” Total fluorescence did not change over the course of the titration, indicating that the fluorescein tag did not interfere with binding. *C*, isothermal titration calorimetry measurements for p180¹⁸⁹⁻³²³ titrated into Mcm10-ID at 21 °C. Upper panel, raw isothermal titration calorimetry data for sequential injections of p180¹⁸⁹⁻³²³; lower panel, integrated heat responses (squares) fit with a single site binding model (continuous line). Best fit parameters for the curve fit were $K_d = 30 \pm 1 \mu$ M, $\Delta H = 0.4$ kcal/mol, and $T\Delta S = 6.5$ kcal/mol. The inset shows the heat effects resulting from successive injections of buffer into protein that was subtracted from binding isotherms.

ID. The strength of the Mcm10-ID-p180¹⁸⁹⁻³²³ interaction was quantified using a fluorescence anisotropy assay. Titration of unlabeled Mcm10-ID into a solution of fluorescein-labeled p180¹⁸⁹⁻³²³ resulted in a robust increase in fluorescence anisotropy, whereas the addition of either ssDNA or buffer alone had no effect (Fig. 2B). Analysis of the titration data by a two-state binding model provided an apparent dissociation constant (K_d) of $12 \pm 2 \mu$ M for Mcm10-ID binding to p180¹⁸⁹⁻³²³. This value is in good agreement with the K_d ($30 \pm 1 \mu$ M) determined by isothermal titration calorimetry using unlabeled proteins (Fig. 2C).

NMR chemical shift perturbation experiments were used to probe the Mcm10-ID and p180¹⁸⁹⁻³²³ interaction in greater detail and map the p180¹⁸⁹⁻³²³ binding site on Mcm10-ID. We previously obtained sequence specific backbone assignments of Mcm10-ID and used chemical shift perturbation to map the DNA binding site (31). Here, we monitored ¹H and ¹⁵N chemical shift perturbations of uniformly ¹⁵N-labeled Mcm10-ID upon the addition of unlabeled p180¹⁸⁹⁻³²³ (Fig. 3A). These experiments revealed a number of significant chemical shift perturbations in the two-dimensional ¹H,¹⁵N HSQC spectrum that mapped onto the OB-fold cleft, with the strongest pertur-

bations observed for residues in β 1, β 2, β 5.1, L12, and L45 (Fig. 3, B and C). In fact, the resulting spectrum for the Mcm10-ID-p180¹⁸⁹⁻³²³ complex is remarkably similar to that previously measured for Mcm10-ID-ssDNA complex (31) (supplemental Fig. S9), suggesting that Mcm10-ID utilizes a common binding site for both ssDNA and p180. Moreover, both p180¹⁸⁹⁻³²³ and ssDNA bind to Mcm10-ID in the fast-to-intermediate-exchange regime, with some peaks gradually shifting over the course of the titration, whereas others broaden and disappear. However, by comparing the magnitude of the chemical shift perturbations in response to p180¹⁸⁹⁻³²³ and ssDNA binding, it appears that Mcm10-ID binds more weakly to p180¹⁸⁹⁻³²³ than to ssDNA (data not shown). This observation is consistent with the 4-fold weaker Mcm10 dissociation constant determined by fluorescence anisotropy ($3 \pm 1 \mu$ M for ssDNA versus $12 \pm 2 \mu$ M for p180¹⁸⁹⁻³²³).

ssDNA and p180¹⁸⁹⁻³²³ Compete for the Same Site on Mcm10-ID—A common binding site for ssDNA and p180 suggests that these two ligands either compete for binding or bind cooperatively to Mcm10. To distinguish between these two possibilities,

competition experiments were performed utilizing NMR chemical shift perturbations to monitor the interaction of p180¹⁸⁹⁻³²³ and ssDNA with Mcm10-ID (Fig. 4A, supplemental Fig. S5A). First, ssDNA was titrated into a sample containing ¹⁵N-labeled Mcm10-ID, and peak shifts were observed as previously reported (Fig. 4A, red spectrum) (31). Next, unlabeled p180¹⁸⁹⁻³²³ was titrated into the same sample containing ssDNA-saturated Mcm10-ID (Fig. 4A, green spectrum). No further chemical shift perturbations were observed with the addition of protein, which suggests that p180¹⁸⁹⁻³²³ neither interacts with an Mcm10-ID-ssDNA complex nor does it displace ssDNA from Mcm10-ID.

To test whether ssDNA is able to disrupt a preformed Mcm10-ID-p180¹⁸⁹⁻³²³ complex, the reverse titration was performed in which unlabeled p180¹⁸⁹⁻³²³ was first added to a sample containing ¹⁵N-labeled Mcm10-ID followed by the addition of ssDNA (Fig. 4B, supplemental Fig. S5B). As in Fig. 3, the addition of p180¹⁸⁹⁻³²³ to ¹⁵N-labeled Mcm10-ID resulted in significant perturbation in chemical shifts for a discrete set of residues (Fig. 4B, blue spectrum). Upon the addition of ssDNA, the peaks that were perturbed by p180¹⁸⁹⁻³²³ changed trajectory and shifted to resemble the Mcm10-ID-ssDNA spectrum (Fig. 4B, gold spectrum).

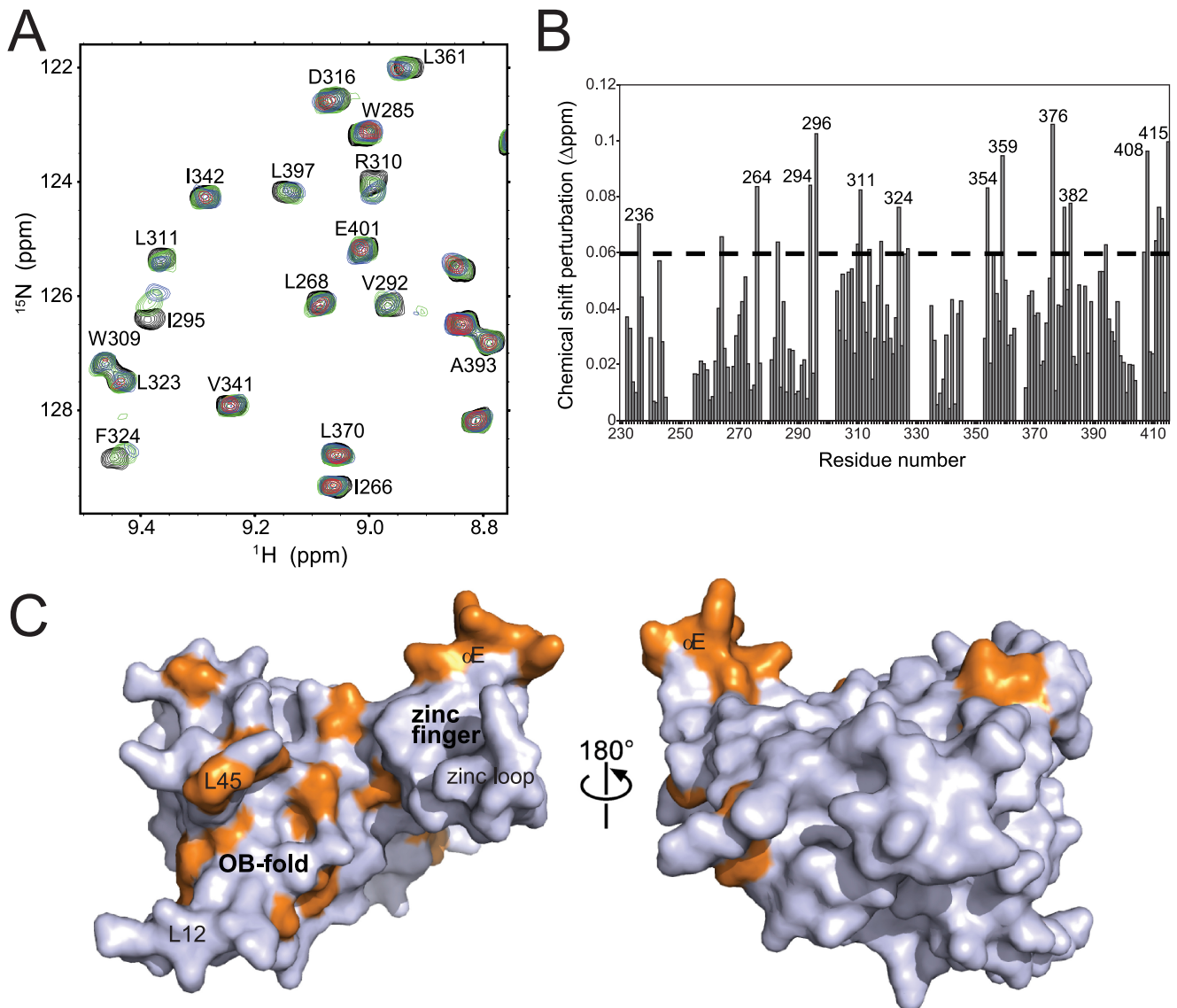


FIGURE 3. **Mapping the p180¹⁸⁹⁻³²³ binding site onto Mcm10-ID.** *A*, an overlay of a region of ^1H , ^{15}N HSQC spectra of ^{15}N -enriched Mcm10-ID in response to the addition of p180¹⁸⁹⁻³²³, with the peak assignments labeled. The titration was performed at Mcm10-ID:p180¹⁸⁹⁻³²³ ratios of 1:0 (black), 1:0.25 (green), 1:0.67 (blue), and 1:1 (red). *B*, quantitation of chemical shift perturbations from the addition of equimolar amounts of Mcm10-ID and p180¹⁸⁹⁻³²³ (see "Experimental Procedures"). The dashed line denotes 1 S.D. above the mean. A shift of zero indicates an unassigned residue. *C*, surface representation of Mcm10-ID with the residues exhibiting a significant shift (above the dashed line in panel *B*) colored orange. The 180° rotation illustrates that the shifts occur almost exclusively on the ssDNA binding face of the protein.

To test the ability of ssDNA to displace Mcm10 from p180, we performed a NMR titration in which Mcm10-ID and ssDNA were added in succession to a solution containing ^{15}N -enriched p180¹⁸⁹⁻³²³. When Mcm10-ID was titrated into ^{15}N -p180¹⁸⁹⁻³²³, displacement of a discrete number of chemical shifts was observed, indicative of formation of the Mcm10-ID·p180 complex (Fig. 4C, supplemental Fig. S6A, blue spectrum). The addition of ssDNA to the protein complex caused the chemical shifts to revert to their starting location in the spectrum of ^{15}N -p180¹⁸⁹⁻³²³ alone (Fig. 4C, gold). This directly demonstrates that ssDNA is capable of displacing Mcm10-ID from p180¹⁸⁹⁻³²³. A fourth titration was performed in which ssDNA was first added into the ^{15}N -labeled p180¹⁸⁹⁻³²³ sample. In this case no peak shifts were observed, indicating that p180¹⁸⁹⁻³²³ does not bind ssDNA (Fig. 4D, supplemental Fig. S6B, green spectrum). When

Mcm10-ID was titrated into this sample containing free p180¹⁸⁹⁻³²³ and ssDNA, perturbation of p180 chemical shifts that mimicked the ^{15}N -p180¹⁸⁹⁻³²³/Mcm10-ID spectrum were observed (compare the blue spectrum in Fig. 4C with the red spectrum in Fig. 4D). However, the magnitude of Mcm10-ID-induced ^{15}N -p180¹⁸⁹⁻³²³ peak shifts in the presence of ssDNA were not as large as those in the absence of ssDNA, consistent with a partitioning of Mcm10 between both p180¹⁸⁹⁻³²³ and ssDNA. Taken together, these data demonstrate that ssDNA and p180¹⁸⁹⁻³²³ compete for binding to the OB-fold cleft of Mcm10-ID and that ssDNA is able to displace p180¹⁸⁹⁻³²³ from Mcm10-ID, consistent with the moderate preference of Mcm10-ID for ssDNA over p180¹⁸⁹⁻³²³.

To quantify the competition of ssDNA and p180¹⁸⁹⁻³²³ for Mcm10-ID, we examined the concentration dependence on the displacement reaction using the fluorescence anisotropy assay

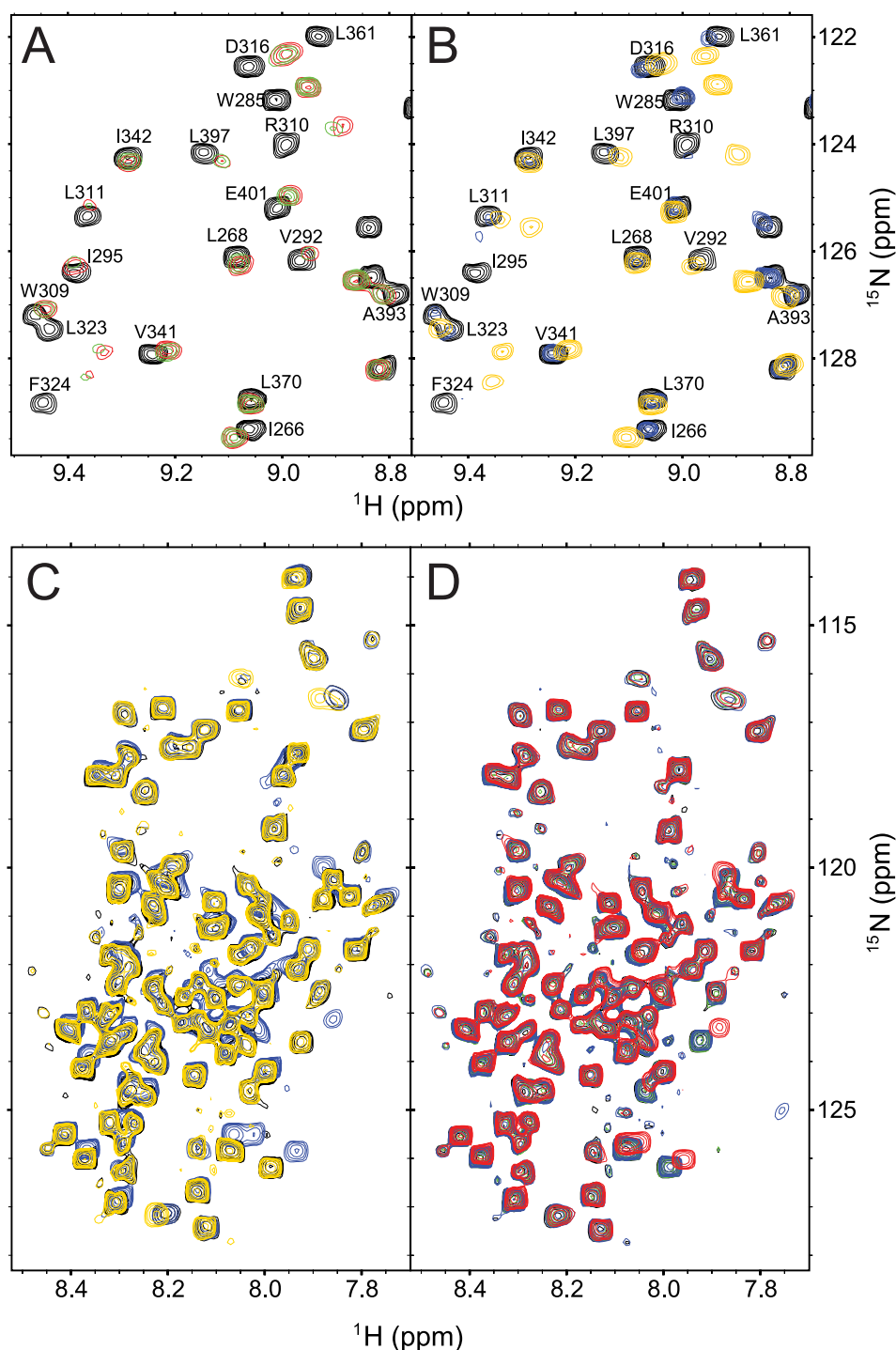


FIGURE 4. **Competition for Mcm10-ID binding by ssDNA and p180^{189–323}.** A, NMR chemical shift perturbations in response to ssDNA and p180^{189–323} binding to ¹⁵N-enriched Mcm10-ID. The region of the overlaid spectra is the same as in Fig. 3A, with Mcm10-ID alone (black), 1:1 ratio of Mcm10-ID:ssDNA (red), and a 1:1:1 ratio of Mcm10-ID:ssDNA:p180^{189–323} (green). B, the reverse titration with the same overlay region of the ¹H,¹⁵N HSQC spectra as before. Mcm10-ID alone (black) was mixed in a 1:1 ratio of p180^{189–323} (blue), then ssDNA was added to this mixture in a 1:1:1 ratio (gold). C, reciprocal titrations from panels A and B, performed with ¹⁵N-enriched p180^{189–323} (black), a 1:1 molar ratio of p180^{189–323}:Mcm10-ID (blue), and a 1:1:1 ratio of p180^{189–323}:Mcm10-ID:ssDNA (gold). D, the reverse titration as in panel C with p180^{189–323} alone (black), a 1:1 molar ratio of p180^{189–323}:ssDNA (green), a 1:1:0.67 molar ratio of p180^{189–323}:ssDNA:Mcm10-ID (blue), and then a 1:1:1 molar ratio of ¹⁵N-p180^{189–323}:ssDNA:Mcm10-ID (red).

(Fig. 5). In separate experiments Mcm10-ID·fluorescein-ssDNA and Mcm10-ID·fluorescein-p180^{189–323} complexes were assembled, and the decay in fluorescence anisotropy was plotted as

increasing amounts of unlabeled competitor was added. Upon the addition of ssDNA to Mcm10-ID·fluorescein-p180^{189–323}, we observed a return in the anisotropy signal back to within 15% that of free fluorescein-p180^{189–323}, demonstrating a robust displacement of p180^{189–323} from Mcm10 by ssDNA. The calculated K_i for this reaction is $2.8 \pm 0.2 \mu\text{M}$, roughly equal to the K_d for the Mcm10-ID:ssDNA interaction ($3.4 \pm 0.5 \mu\text{M}$). Conversely, the addition of p180^{189–323} to Mcm10·fluorescein-ssDNA complexes reduced the anisotropy signal only $\sim 30\%$, even at the highest concentration of p180 tested ($K_i > 50 \mu\text{M}$), indicating that p180^{189–323} only weakly competes for binding. These results are fully consistent with the chemical shift perturbation experiments described above.

The Minimal Mcm10-ID Binding Site Maps to p180^{286–310}—To map the minimal region of p180^{189–323} needed to interact with Mcm10-ID, the p180 sequence was aligned and examined for conservation and predicted secondary structure. In addition, the data from the ¹H,¹⁵N HSQC titration of ¹⁵N-labeled p180^{189–323} with unlabeled Mcm10-ID (supplemental Fig. S6) was carefully examined to determine whether insights could be obtained into the location of the Mcm10-ID binding site on p180^{189–323}, even in the absence of sequence specific assignments, following the strategy described previously (52). The key to this approach is to monitor the total number of resonances perturbed in the titration and take advantage of the unique chemical shifts of the glycine backbone and glutamine and asparagine side chain amides. Analysis of the data in this way suggests that the binding sequence should contain ~ 20 residues including at least one glycine and no asparagine or glutamine residues. In the sequence of p180^{189–323}, only two peptides fit these criteria, p180^{243–256} and p180^{286–310}. Indeed, glutathione-immobilized GST-p180^{243–310}, which spanned both peptides, was able to capture Mcm10-ID from solution in our affinity chromatography assay (Fig. 2A). To

assess which peptide contains the Mcm10-ID binding sequence, the individual p180^{243–256} and p180^{286–310} peptides were synthesized and used in chemical shift perturbation experiments with ¹⁵N-enriched Mcm10-ID. Of the two peptides, only p180^{286–310} induced significant chemical shift perturbations in Mcm10-ID that resembled those of p180^{189–323} (Fig. 6A, supplemental Fig. S9). Binding of p180^{286–310} occurred on the fast-exchange timescale and resulted in a magnitude of chemical shift perturbations similar to those caused by p180^{189–323} (supplemental Fig. S7). These data show that p180 residues 286–310 bind to the same region of Mcm10-ID as p180^{189–323} and ssDNA (Fig. 6, B and C) and are consistent with the relative binding affinities for p180^{189–323} ($K_d = 12 \pm 2 \mu\text{M}$) and p180^{286–310} ($K_d = 32 \pm 2 \mu\text{M}$) measured by fluorescence anisotropy (supplemental Fig. S7D).

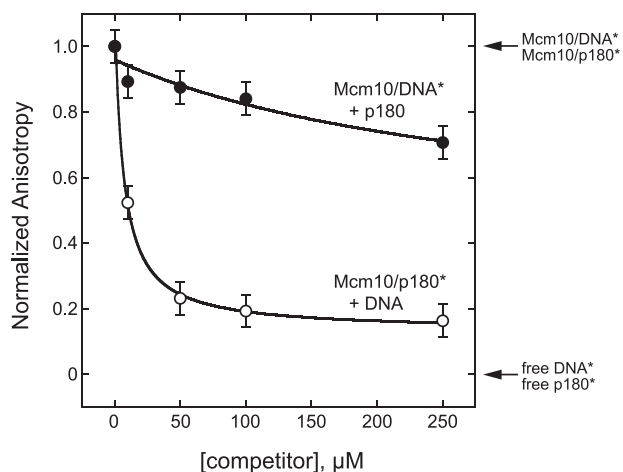


FIGURE 5. Quantitation of p180^{189–323} and ssDNA displacement from Mcm10-ID. The decay in fluorescence anisotropy was monitored as unlabeled ssDNA was added to preformed Mcm10-ID-fluorescein-p180^{189–323} complexes (open circles) and as unlabeled p180^{189–323} was added to preformed Mcm10-ID-fluorescein-ssDNA complexes (closed circles). Mcm10-ID and fluorescein-labeled molecules (DNA*, p180*) were held at 15 μM and 50 nM, respectively. Anisotropy (r) values were normalized to correct for the differences in signal between DNA* and p180*, in which $r = 0$ reflects the anisotropy for free DNA* and p180* (before the addition of Mcm10-ID), and $r = 1$ reflects the anisotropy for Mcm10-ID-ssDNA* and Mcm10-ID-p180* before the addition of unlabeled competitor.

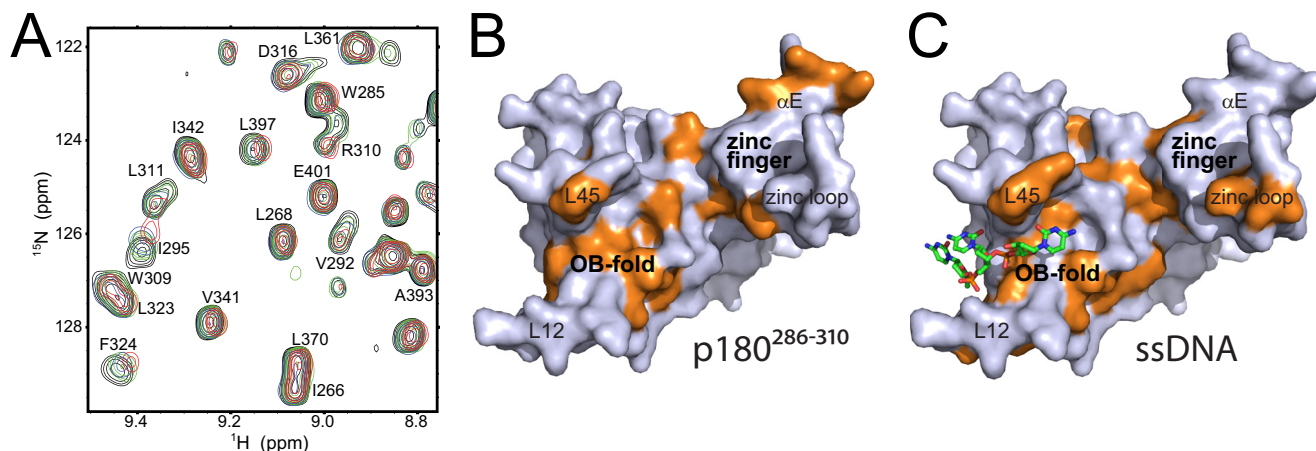


FIGURE 6. Mapping the p180^{286–310} binding site into Mcm10. A, overlay of a representative section of the ¹H, ¹⁵N HSQC spectra from ¹⁵N-enriched Mcm10-ID performed at Mcm10-ID:p180^{286–310} ratios of 1:0 (black), 1:0.25 (green), 1:0.5 (blue), and 1:1 (red). B, surface representation of Mcm10-ID showing that residues exhibiting a significant shift in response to p180^{286–310} (orange) predominate on the ssDNA binding face of the protein. L12 loop residues 297–302 were not assigned in the NMR spectra. C, the Mcm10-ID-ssDNA co-crystal structure, with NMR chemical shift perturbations from titration with ssDNA highlighted orange (data are from Ref. 31).

Mcm10-ID+CTD Binds ssDNA and p180^{189–323}—Having thoroughly characterized the binding of ssDNA and p180 to Mcm10-ID, we asked how studies of the isolated domain relate to the biochemical functions of the intact protein. Mcm10-CTD has previously been shown to bind both DNA and p180^{1–323} (29). The linking of the ID and CTD are, therefore, anticipated to result in higher affinity and possibly altered specificity. To this end, a protein deletion construct encompassing Mcm10-ID and -CTD was constructed, purified, and characterized by biochemical approaches.

Binding of Mcm10-ID+CTD to various DNA substrates designed to resemble replication intermediates was measured by fluorescence anisotropy (Table 2). The goal of these experiments was to test the effects of DNA structure and length under identical conditions and to compare the relative affinities between DNA and p180 (see below). Mcm10-ID+CTD bound all DNAs tested with 10-fold greater affinity than previously determined for ID or CTD alone. This observation is similar to our previous results obtained with a maltose-binding protein-tagged full-length Mcm10 (29). Additionally, the ID+CTD protein bound ssDNA with a slightly higher affinity than dsDNA when tested against both 25- and 45-mer oligonucleotides, as observed previously for the isolated domains and the intact protein (28, 29, 31) (Table 2). Moreover, Mcm10-ID+CTD does not demonstrate a significant preference for ssDNA, dsDNA, or constructs containing ss/dsDNA junctions, including 5'- and 3'-overhangs, fork, and bubble substrates (Table 2). This lack of specificity for a particular DNA structure was observed previously for the isolated ID and CTD. Thus, together these two binding modules enhance the strength of the DNA interaction but do not provide additional specificity.

Binding of Mcm10-ID+CTD to p180^{189–323} was investigated by fluorescence anisotropy using fluorescein-tagged p180^{189–323} protein. Mcm10-ID+CTD bound to fluorescein-p180^{189–323} with a K_d of $0.19 \pm 0.03 \mu\text{M}$ (Table 2). The strength of the Mcm10-ID+CTD interaction with p180^{189–323} is ~50-fold greater than that measured for Mcm10-ID alone ($K_d = 12 \pm 2 \mu\text{M}$). Importantly, the affinity observed for this tandem

TABLE 2
Mcm10-ID+CTD binding to DNA and pol α -p180^{189–323}

	K_d^a	Relative affinity ^b	DNA sequence ^c
	μM		
ssDNA 25-mer	0.22 \pm 0.05	1.0	5'-ATGGTAGGCAACCATGTAGTAGTCA*
dsDNA 25-mer	0.91 \pm 0.10	0.2	5'-ATGGTAGGCAACCATGTAGTAGTCA* TACCATCCGTTGGTACATCATCAGT-5'
ssDNA 45-mer	0.12 \pm 0.02 (4.30 \pm 1.12)	1.8 (0.05)	5'-GGTAGGCACGAACCATGTAGTAGTAGGCAATCAGCATTTGATAGC*
dsDNA 45-mer	0.40 \pm 0.08 (34.86 \pm 8.70)	0.6 (0.01)	5'-GGTAGGCACGAACCATGTAGTAGTAGGCAATCAGCATTTGATAGC* CCATCCGTGCTTGGTACATCATCACCCTTAGTCGTAACATATCG-5'
Fork	0.11 \pm 0.01	2.0	5'-GGTAGGCACGA AACCATGTAGTAGTA * CCATCCGTGCA ATGATGATGTACCAA -5'
Bubble	0.06 \pm 0.003	3.7	5'-GGTAGGCACGA AACCATGTAGTAGTA AGGCAATCAGC* CCATCCGTGCA ATGATGATGTACCAA CCGTTAGTCG-5'
5'-overhang	0.11 \pm 0.01	2.0	5'-TGACTACTACATGGT *ACTGATGATGTACCA ACGGATGGTA -5'
3'-overhang	0.05 \pm 0.004	4.4	5'-ATGGTTGCCTACCAT * ACTGATGATGTACCAACGGATGGTA -5'
p180 ^{189–323}	0.19 \pm 0.03	1.2	

^a Values were determined by fluorescence anisotropy as described under "Experimental Procedures." Values in parentheses were recorded at 300 mM NaCl; all others were at 150 mM NaCl.

^b Binding affinities relative to ssDNA 25-mer.

^c ssDNA regions of ss/dsDNA hybrids are in boldface.

construct brings the strength of binding of p180 to the same level as for ssDNA (Table 2). This has important implications for how Mcm10 might recruit p180 (and therefore pol α) to the active replication machinery.

DISCUSSION

Chemical Nature of Mcm10-ID Interactions with DNA and Pol α —In this study we show that both ssDNA and the N-terminal region of p180 compete for binding to a relatively hydrophobic surface within the OB-fold cleft of Mcm10. Our previous analysis showed that in addition to the OB-fold, ssDNA binds to the highly basic extended loop on the zinc finger motif (31). In the structure of the Mcm10-ssDNA complex, the crystal lattice prevented DNA access to the zinc loop, which precluded direct visualization of the interaction between DNA and the zinc finger. However, additional information regarding the nature of intermolecular Mcm10-ID interactions can be inferred from thermodynamic information derived from isothermal titration calorimetry measurements. Titration of Mcm10-ID with ssDNA (supplemental Fig. S2B) revealed an enthalpy-driven, spontaneous reaction ($\Delta H = -9.8$ kcal/mol, $T\Delta S = -3.6$ kcal/mol). This is consistent with our previous mutational analysis that showed electrostatic interactions play a large role in ssDNA binding to Mcm10-ID (31). Taking the structural and biochemical data together, binding of ssDNA to Mcm10-ID is largely mediated by hydrophobic residues located within the OB-fold cleft as well as by polar/charged residues located on the L12 and L45 loops (e.g. Ser-299) between the OB-fold and the zinc finger (Lys-293) and on the zinc loop (Lys-385 and Lys-386). In contrast, calorimetric titration of Mcm10-ID with p180^{189–323} (Fig. 2C) revealed a large entropic contribution ($\Delta H = 0.4$ kcal/mol; $T\Delta S = 6.5$ kcal/mol), suggesting that hydrophobic interactions may be important to the protein-protein interaction. Indeed, p180^{189–323} and p180^{286–310} binding mapped to the aliphatic OB-fold cleft. Interestingly, NMR chemical shifts corresponding to basic residues on the zinc finger helix (αE) and not the DNA binding zinc loop were perturbed by all three p180 constructs tested, including p180^{243–256}, which did not bind to the OB-fold (supplemental

Fig. S9). Thus, we speculate that a hydrophobic interaction at the OB-fold may provide additional specificity for p180^{286–310}.

Pol α and Mcm10 Binding Domains—The overall domain structure of p180 is known, and the activities of the central polymerase and the C-terminal subunit assembly domains have been characterized (53, 54). However, the function of the N-terminal domain is less clear. This region of p180 is dispensable for polymerase activity and is not required for assembly of the pol α -primase complex. The N terminus of p180 is phosphorylated by cyclin A-dependent kinase 2 on residues 174, 209, and 219 (55, 56), and it interacts with several proteins of various functions including Mcl1 (And-1/Ctf4) (57), PP2A (56), concanavalin A and *Ricinus communis* agglutinin I (58), SV40 Large T-antigen (59, 60), and Mcm10 (29). Although the importance of these interactions has yet to be determined, our observation that Mcm10 interacts with p180^{286–310} outside of the polymerase domain is consistent with Mcm10 anchoring the pol α complex onto DNA in such a way as to not interfere with RNA or DNA synthesis.

The finding that Mcm10-ID interacts with both ssDNA and pol α through contacts in the OB-fold domain reflects the adaptability of this motif to bind a range of different biological molecules. This cleft is used by various proteins to engage RNA (61), DNA (46), oligosaccharides (62), proteins (63), and even metals and inorganic phosphates (64, 65). For example, RPA, a eukaryotic recruiting and scaffolding protein critical to DNA replication, has been shown to bind both oligonucleotides and peptides through its six OB-fold domains (66–70). Mcm10 appears to exhibit similar behavior by binding to DNA, pol α , Dbf4-dependent kinase, and PCNA (24, 25, 31), although the role of the OB-fold in Mcm10 interactions with Dbf4-dependent kinase and PCNA remains to be determined.

A Molecular Mechanism for Mcm10 Hand-off of Pol α to DNA—This is the first report of competition between DNA and pol α for binding to Mcm10. Competition for sites provides a ready mechanism for direct coupling of the protein interaction with DNA binding as a means to promote progression of the replication machinery. Although the exact role of Mcm10 in replication initiation has yet to be elucidated, it is reasonable to

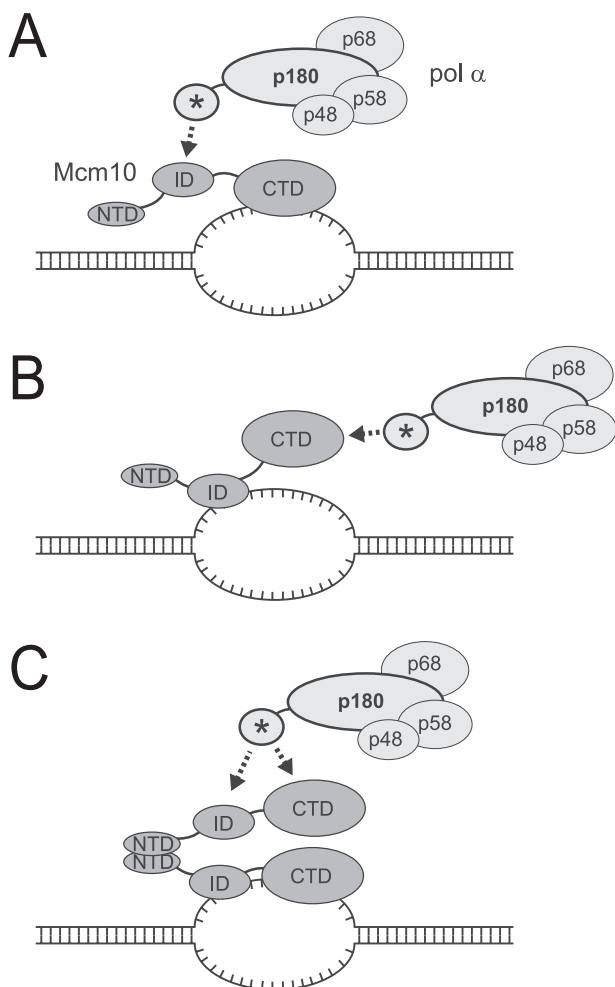


FIGURE 7. Three possible modes of Mcm10 binding to ssDNA and pol α at a replication fork. Mcm10-ID (A) and Mcm10-CTD (B) form binary complexes with either DNA or the N-terminal region of p180 (labeled with an asterisk). C, the ID+CTD together bind DNA and p180 with higher affinity than either the ID or CTD alone. Oligomerization via the NTD could also allow the ID and CTD from one subunit to contact DNA, while a second subunit recruits pol α .

envison Mcm10 as a macromolecular recruiting and/or scaffolding protein because of the fact that Mcm10 contains two domains that can bind to DNA and pol α (29). This follows a common strategy for numerous modular proteins involved in DNA processing; there is a significant kinetic advantage to deconstructing protein interactions into two or more weak binding sites (68). The recruitment of pol α to origins of replication by Mcm10 would be a significant step to signal nascent DNA synthesis and contribute to fork stability (6, 12, 16, 24, 26, 27, 29, 71). Indeed, Mcm10 has been shown to be necessary for pol α loading onto chromatin (4).

The detailed analysis of binding affinities and competition experiments presented here demonstrate that the highly conserved Mcm10-ID transitions between interaction with DNA and pol α , consistent with an Mcm10-mediated hand-off mechanism (Fig. 7). The relatively similar affinities of p180^{189–323} and ssDNA for Mcm10-ID+CTD suggest that full-length Mcm10 also partitions between DNA and pol α binding. Two scenarios for hand-off of pol α onto DNA by a single Mcm10 molecule can be envisioned, the first in which the CTD interacts with ssDNA as the ID engages p180^{286–310} (Fig. 7A). Equiv-

alently, Mcm10 could bind to the DNA through the ID, while the CTD tethers the N-terminal region of p180 (Fig. 7B). It is interesting to note that binding of p180^{189–323} to CTD alone was undetectable by our fluorescence assay (data not shown), raising the possibilities that either the CTD binds to p180^{1–323} outside of the 189–323 subdomain or that the CTD indirectly stimulates binding of Mcm10-ID to p180. Indeed, Mcm10-ID+CTD binds both ssDNA and p180^{189–323} with 15-fold greater affinity than Mcm10-ID alone, suggesting that protein and DNA binding can be modified by domain interactions within Mcm10. However, anisotropy binding studies carried out with a mixture of Mcm10-ID and Mcm10-CTD did not enhance the binding affinity relative to either domain alone, and thus far we have been unable to observe a direct interaction between the ID and CTD. An alternate interpretation for the enhanced binding with the Mcm10-ID+CTD construct is that a second binding site on the CTD provides an extended interaction surface for DNA, which results in a synergistic effect on binding similar to that observed for the multiple OB-fold binding motifs in RPA (72).

Mcm10 oligomerization provides a third mechanism for mediating DNA and p180 binding (Fig. 7C). Mcm10 has been reported to form dimeric and hexameric assemblies (25, 73). We previously showed that Mcm10-NTD, which is predicted to contain a coiled-coil motif, forms a highly asymmetric dimer in solution (29). Dimerization of Mcm10 through the NTD would expose multiple ID+CTD high affinity binding platforms for binding to DNA and/or pol α . The higher affinity of the ID+CTD construct for both ssDNA and p180^{189–323} suggests that this is the preferred binding mode over the individual domains. Importantly, the similar affinities of Mcm10-ID+CTD for pol α and DNA provides a physical basis for simultaneous binding of ssDNA and pol α by Mcm10. This condition also raises the possibility that a structural change would be necessary to facilitate Mcm10 release of pol α during a molecular handoff to DNA. Previous studies suggest that phosphorylation (74) or ubiquitination (24) are likely candidates for altering Mcm10 binding affinities. Additional studies beyond the scope of this paper, including elucidating the structure of full-length Mcm10 and determining interaction partners, are required to fully understand how Mcm10 mediates critical interactions at the eukaryotic replication fork.

Acknowledgments—We gratefully acknowledge Sivaraja Vaithiyalingam for assistance with NMR experiments and thank the staff at beamlines 21-ID at the Advanced Photon Source (Argonne National Laboratory, Argonne, IL) and the RapiData, X3A, and X29A staff at the National Synchrotron Light Source (Brookhaven National Laboratory, Upton, NY). Use of the Advanced Photon Source was supported by the United States Dept. of Energy Office of Basic Energy Sciences under Contract DE-AC02-06CH11357. Use of LS-CAT Sector 21 was supported by the Michigan Economic Development Corp. and the Michigan Technology Tri-Corridor for the support of this research program (Grant 08SP1000817). Additional thanks go to Haijiang Zhang for preliminary Mcm10-p180^{189–323} binding data.

REFERENCES

- Arias, E. E., and Walter, J. C. (2007) *Genes Dev.* **21**, 497–518
- Solomon, N. A., Wright, M. B., Chang, S., Buckley, A. M., Dumas, L. B., and Gaber, R. F. (1992) *Yeast* **8**, 273–289
- Merchant, A. M., Kawasaki, Y., Chen, Y., Lei, M., and Tye, B. K. (1997) *Mol. Cell. Biol.* **17**, 3261–3271
- Wohlschlegel, J. A., Dhar, S. K., Prokhorova, T. A., Dutta, A., and Walter, J. C. (2002) *Mol. Cell* **9**, 233–240
- Pacek, M., and Walter, J. C. (2004) *EMBO J.* **23**, 3667–3676
- Pacek, M., Tutter, A. V., Kubota, Y., Takisawa, H., and Walter, J. C. (2006) *Mol. Cell* **21**, 581–587
- Moyer, S. E., Lewis, P. W., and Botchan, M. R. (2006) *Proc. Natl. Acad. Sci. U.S.A.* **103**, 10236–10241
- Gambus, A., Jones, R. C., Sanchez-Diaz, A., Kanemaki, M., van Deursen, F., Edmondson, R. D., and Labib, K. (2006) *Nat. Cell Biol.* **8**, 358–366
- Tanaka, T., and Nasmyth, K. (1998) *EMBO J.* **17**, 5182–5191
- Zou, L., and Stillman, B. (2000) *Mol. Cell. Biol.* **20**, 3086–3096
- Walter, J., and Newport, J. (2000) *Mol. Cell* **5**, 617–627
- Zhu, W., Ukomadu, C., Jha, S., Senga, T., Dhar, S. K., Wohlschlegel, J. A., Nutt, L. K., Kornbluth, S., and Dutta, A. (2007) *Genes Dev.* **21**, 2288–2299
- Zegeerman, P., and Diffley, J. F. (2007) *Nature* **445**, 281–285
- Tanaka, S., Umemori, T., Hirai, K., Muramatsu, S., Kamimura, Y., and Araki, H. (2007) *Nature* **445**, 328–332
- Garg, P., and Burgers, P. M. (2005) *Crit. Rev. Biochem. Mol. Biol.* **40**, 115–128
- Ricke, R. M., and Bielinsky, A. K. (2004) *Mol. Cell* **16**, 173–185
- Nasmyth, K., and Nurse, P. (1981) *Mol. Gen. Genet.* **182**, 119–124
- Maine, G. T., Sinha, P., and Tye, B. K. (1984) *Genetics* **106**, 365–385
- Kawasaki, Y., Hiraga, S., and Sugino, A. (2000) *Genes Cells* **5**, 975–989
- Izumi, M., Yanagi, K., Mizuno, T., Yokoi, M., Kawasaki, Y., Moon, K. Y., Hurwitz, J., Yatagai, F., and Hanaoka, F. (2000) *Nucleic Acids Res.* **28**, 4769–4777
- Hart, E. A., Bryant, J. A., Moore, K., and Aves, S. J. (2002) *Curr. Genet.* **41**, 342–348
- Christensen, T. W., and Tye, B. K. (2003) *Mol. Biol. Cell* **14**, 2206–2215
- Homesley, L., Lei, M., Kawasaki, Y., Sawyer, S., Christensen, T., and Tye, B. K. (2000) *Genes Dev.* **14**, 913–926
- Das-Bradoo, S., Ricke, R. M., and Bielinsky, A. K. (2006) *Mol. Cell. Biol.* **26**, 4806–4817
- Lee, J. K., Seo, Y. S., and Hurwitz, J. (2003) *Proc. Natl. Acad. Sci. U.S.A.* **100**, 2334–2339
- Ricke, R. M., and Bielinsky, A. K. (2006) *J. Biol. Chem.* **281**, 18414–18425
- Chattopadhyay, S., and Bielinsky, A. K. (2007) *Mol. Biol. Cell* **18**, 4085–4095
- Fien, K., Cho, Y. S., Lee, J. K., Raychaudhuri, S., Tappin, I., and Hurwitz, J. (2004) *J. Biol. Chem.* **279**, 16144–16153
- Robertson, P. D., Warren, E. M., Zhang, H., Friedman, D. B., Lary, J. W., Cole, J. L., Tutter, A. V., Walter, J. C., Fanning, E., and Eichman, B. F. (2008) *J. Biol. Chem.* **283**, 3338–3348
- Fien, K., and Hurwitz, J. (2006) *J. Biol. Chem.* **281**, 22248–22260
- Warren, E. M., Vaithiyalingam, S., Haworth, J., Greer, B., Bielinsky, A. K., Chazin, W. J., and Eichman, B. F. (2008) *Structure* **16**, 1892–1901
- D'Urso, G., Grallert, B., and Nurse, P. (1995) *J. Cell Sci.* **108**, 3109–3118
- LaRocque, J. R., Dougherty, D. L., Hussain, S. K., and Sekelsky, J. (2007) *Genetics* **176**, 1441–1451
- Wang, T. S. (1991) *Annu. Rev. Biochem.* **60**, 513–552
- Arezi, B., and Kuchta, R. D. (2000) *Trends Biochem. Sci.* **25**, 572–576
- Foiani, M., Marini, F., Gamba, D., Lucchini, G., and Plevani, P. (1994) *Mol. Cell. Biol.* **14**, 923–933
- Ott, R. D., Rehfuess, C., Podust, V. N., Clark, J. E., and Fanning, E. (2002) *Mol. Cell. Biol.* **22**, 5669–5678
- Kunkel, T. A., and Burgers, P. M. (2008) *Trends Cell Biol.* **18**, 521–527
- Otwinowski, Z., and Minor, W. (1997) *Methods Enzymol.* **276**, 307–326
- Vagin, A., and Teplyakov, A. (1997) *J. Appl. Crystallogr.* **30**, 1022–1025
- Brünger, A. T., Adams, P. D., Clore, G. M., DeLano, W. L., Gros, P., Grosse-Kunstleve, R. W., Jiang, J. S., Kuszewski, J., Nilges, M., Pannu, N. S., Read, R. J., Rice, L. M., Simonson, T., and Warren, G. L. (1998) *Acta Crystallogr. D. Biol. Crystallogr.* **54**, 905–921
- Afonine, P. V., Grosse-Kunstleve, R. W., and Adams, P. D. (2005) *Acta Crystallogr. D. Biol. Crystallogr.* **61**, 850–855
- Emsley, P., and Cowtan, K. (2004) *Acta Crystallogr. D. Biol. Crystallogr.* **60**, 2126–2132
- Painter, J., and Merritt, E. A. (2006) *Acta Crystallogr. D. Biol. Crystallogr.* **62**, 439–450
- Laskowski, R. A., MacArthur, M. W., Moss, D. S., and Thornton, J. M. (1993) *J. Appl. Crystallogr.* **26**, 283–291
- Bochkarev, A., Pfuetzner, R. A., Edwards, A. M., and Frappier, L. (1997) *Nature* **385**, 176–181
- Bogden, C. E., Fass, D., Bergman, N., Nichols, M. D., and Berger, J. M. (1999) *Mol. Cell* **3**, 487–493
- Raghunathan, S., Kozlov, A. G., Lohman, T. M., and Waksman, G. (2000) *Nat. Struct. Biol.* **7**, 648–652
- Singleton, M. R., Scaife, S., and Wigley, D. B. (2001) *Cell* **107**, 79–89
- Lee, T. T., Agarwalla, S., and Stroud, R. M. (2005) *Cell* **120**, 599–611
- Bhattacharya, S., Arunkumar, A. I., Sullivan, S. L., Botuyan, M. V., Arrowsmith, C. H., and Chazin, W. J. (2004) *J. Biomol. NMR* **28**, 195–196
- Mer, G., Bochkarev, A., Gupta, R., Bochkareva, E., Frappier, L., Ingles, C. J., Edwards, A. M., and Chazin, W. J. (2000) *Cell* **103**, 449–456
- Mizuno, T., Yamagishi, K., Miyazawa, H., and Hanaoka, F. (1999) *Mol. Cell. Biol.* **19**, 7886–7896
- Muzi-Falconi, M., Giannattasio, M., Foiani, M., and Plevani, P. (2003) *ScientificWorldJournal* **3**, 21–33
- Nasheuer, H. P., Moore, A., Wahl, A. F., and Wang, T. S. (1991) *J. Biol. Chem.* **266**, 7893–7903
- Schub, O., Rohaly, G., Smith, R. W., Schneider, A., Dehde, S., Dornreiter, I., and Nasheuer, H. P. (2001) *J. Biol. Chem.* **276**, 38076–38083
- Williams, D. R., and McIntosh, J. R. (2005) *Eukaryot. Cell* **4**, 166–177
- Hsi, K. L., Copeland, W. C., and Wang, T. S. (1990) *Nucleic Acids Res.* **18**, 6231–6237
- Dornreiter, I., Copeland, W. C., and Wang, T. S. (1993) *Mol. Cell. Biol.* **13**, 809–820
- Taneja, P., Nasheuer, H. P., Hartmann, H., Grosse, F., Fanning, E., and Weisshart, K. (2007) *Biochem. J.* **407**, 313–320
- Berthet-Colominas, C., Seignovet, L., Härtlein, M., Grotli, M., Cusack, S., and Leberman, R. (1998) *EMBO J.* **17**, 2947–2960
- Stein, P. E., Boodhoo, A., Armstrong, G. D., Cockle, S. A., Klein, M. H., and Read, R. J. (1994) *Structure* **2**, 45–57
- Bochkareva, E., Belegu, V., Korolev, S., and Bochkarev, A. (2001) *EMBO J.* **20**, 612–618
- Hall, D. R., Gourley, D. G., Leonard, G. A., Duke, E. M., Anderson, L. A., Boxer, D. H., and Hunter, W. N. (1999) *EMBO J.* **18**, 1435–1446
- Heikinheimo, P., Lehtonen, J., Baykov, A., Lahti, R., Cooperman, B. S., and Goldman, A. (1996) *Structure* **4**, 1491–1508
- Lee, J. H., Park, C. J., Arunkumar, A. I., Chazin, W. J., and Choi, B. S. (2003) *Nucleic Acids Res.* **31**, 4747–4754
- Daughdrill, G. W., Buchko, G. W., Botuyan, M. V., Arrowsmith, C., Wold, M. S., Kennedy, M. A., and Lowry, D. F. (2003) *Nucleic Acids Res.* **31**, 4176–4183
- Stauffer, M. E., and Chazin, W. J. (2004) *J. Biol. Chem.* **279**, 25638–25645
- Bochkareva, E., Kaustov, L., Ayed, A., Yi, G. S., Lu, Y., Pineda-Lucena, A., Liao, J. C., Okorokov, A. L., Milner, J., Arrowsmith, C. H., and Bochkarev, A. (2005) *Proc. Natl. Acad. Sci. U.S.A.* **102**, 15412–15417
- Xu, X., Vaithiyalingam, S., Glick, G. G., Mordes, D. A., Chazin, W. J., and Cortez, D. (2008) *Mol. Cell. Biol.* **28**, 7345–7353
- Yang, X., Gregan, J., Lindner, K., Young, H., and Kearsley, S. E. (2005) *BMC Mol. Biol.* **6**, 13
- Arunkumar, A. I., Stauffer, M. E., Bochkareva, E., Bochkarev, A., and Chazin, W. J. (2003) *J. Biol. Chem.* **278**, 41077–41082
- Okorokov, A. L., Waugh, A., Hodgkinson, J., Murthy, A., Hong, H. K., Leo, E., Sherman, M. B., Stoeber, K., Orlova, E. V., and Williams, G. H. (2007) *EMBO Rep.* **8**, 925–930
- Izumi, M., Yatagai, F., and Hanaoka, F. (2001) *J. Biol. Chem.* **276**, 48526–48531